Hearing Research 243 (2008) 1–10

Contents lists available at ScienceDirect

Hearing Research

journal homepage: www.elsevier.com/locate/heares

Methodological paper

Three-dimensional imaging of the intact mouse cochlea by fluorescent laser scanning confocal microscopy

Glen H. MacDonald, Edwin W Rubel *

Virginia Merrill Bloedel Hearing Research Center, Department of Otolaryngology-HNS, University of Washington, Box 357923, Seattle, WA 98195, United States

ARTICLE INFO

Article history:
Received 21 March 2008
Received in revised form 7 May 2008
Accepted 20 May 2008
Available online 6 June 2008

Keywords:
Fluorescence
Confocal
Cochlea
Refractive index
Methyl salicylate
Benzyl benzoate

ABSTRACT

The complex anatomy of the mammalian cochlea is most readily understood by representation in three-dimensions. However, the cochlea is often sectioned to minimize the effects of its anatomic complexity and optical properties on image acquisition by light microscopy. We have found that optical aberrations present in the decalcified cochlea can be greatly reduced by dehydration through graded ethanols followed by clearing with a mixture of five parts methyl salicylate and three parts benzyl benzoate (MSBB). Clearing the cochlea with MSBB enables acquisition of high-resolution images with multiple fluorescent labels, through the full volume of the cochlea by laser scanning confocal microscopy. The resulting images are readily applicable to three-dimensional morphometric analysis and volumetric visualizations. This method promises to be particularly useful for three-dimensional characterization of anatomy, innervation and expression of genes or proteins in the many new animal models of hearing and balance generated by genetic manipulation. Furthermore, the MSBB is compatible with most non-protein fluorophores used for histological labeling, and may be removed with traditional transitional solvents to allow subsequent epoxy embedding for sectioning.

1. Introduction

The use of light microscopy for imaging the auditory and vestibular tissues in the mammalian inner ear faces several challenges. The cochlear shell is among the densest bones in the body, highly scattering to visible light, even after decalcification, and composed of complex spiraling and overlapping structures. The multiple tissue types and fluid-filled spaces within the cochlea combine with its structural complexity to create multiple refractive index (RI) transitions that lead to spherical aberrations.

Serial sections have been traditionally used for high-resolution light microscopy in order to minimize optical aberrations by dividing the organ into a series of essentially two-dimensional (2D) structures. Sections mounted on slides may be imaged without optical aberrations from adjacent tissue structures. However, quantitative and qualitative interpretation of the cochlear anatomy is difficult from 2D images, as is an appreciation of its three-dimensional (3D) structure. Reconstructing the 3D cochlear anatomy from serial sections requires a tedious process of lateral and rotational alignment of images. Although time-consuming, reconstruction of the cochlea from serial sections does allow using high-resolution images acquired by light and electron microscopy (Hashimoto et al., 1990; Liberman et al., 1990; Sato et al., 1999).

More recent approaches to 3D imaging of the cochlea involve computed tomography, magnetic resonance imaging or orthogonal-plane fluorescence optical sectioning (Voie et al., 1993; Voie, 2002). These methods offer benefits over microscopy such as minimal preparation, exceptional imaging depth and wide field of view. However, computed tomography is capable of lateral resolution down to 5–10 μm, but is limited axially to 25 μm (Wang and Vannier, 2001), while magnetic resonance imaging allows somewhat less resolution (Benveniste and Blackband, 2002) and neither method appears optimal for cell-specific labeling. Orthogonal-plane fluorescence optical sectioning has recently achieved a lateral resolution of 5 μm and the ability to distinguish two channels of fluorescence (Voie et al., 2007).

We previously described a novel means to obtain 3D images of the mouse cochlea that employed Spurr's low viscosity resin as a clearing agent in conjunction with pre-embedding immunofluorescence and laser scanning confocal microscopy (Hardie et al., 2004). The epoxy resin also immobilized the cochlear tissues to allow their exposure by bisecting the cochlea along its modiolar axis. This approach allowed images to be readily collected at depths up to 300 μm with 4× objective and to 60 μm with an oil immersion objective.

Here, we describe a simple modification of our prior method that greatly extends the depth to which images may be collected from the intact cochlea. Instead of epoxy resin, we used a mixture of methyl salicylate and benzyl benzoate to render the cochlea

* Corresponding author. Tel.: +1 206 543 8360; fax: +1 206 616 1828.
E-mail address: rubel@u.washington.edu (E. W Rubel).

0378-5955/$ - see front matter © 2008 Elsevier B.V. All rights reserved.
doi:10.1016/j.heares.2008.05.009

exceptionally transparent (Fig. 1). This clearing agent was first employed to image the cochlea by orthogonal-plane fluorescence optical sectioning (Voie et al., 1993). We have found that MSBB allows collecting optical volumes through the entire extent of the cochlea, limited only by the working distance of the objective lens.

2. Methods

2.1. Animals

Cochleas were harvested from 129/CBA mice raised in the University of Washington vivarium in accordance with IACUC regulations. The mice were killed by cervical dislocation at ages from post-natal day 7 (P7) to 6 months and their cochleae exposed by dissection of the temporal bone. After removal of the stapes and opening the round window, a small hole was made in the apex of the cochlea, over the helicotrema, for slow perfusion with 4% paraformaldehyde in 0.1 M sodium–potassium phosphate buffer, pH 7.4. The inner ears were post-fixed by submersion in 4% paraformaldehyde and placed overnight on a rocker at 4 °C.

The specimens were washed with sodium–phosphate buffer containing 0.9% saline, pH 7.4, (PBS) for three changes, 10 min. each, with gentle rocking, at room temperature. A small hole in the cochlear shell was carefully made over the scala vestibuli of the basal turn to facilitate solution exchange during the immunolabeling process. Decalcification was accomplished by submerging in 10% ethylenediamine tetraacetic acid-disodium salt (EDTA) in PBS, pH 7.4, for 4 days at 4 °C, with rocking. The specimens were rinsed free of EDTA with three changes of PBS, for 10 min each, after decalcification.

2.2. Immunolabeling

All steps for immunolabeling were carried out at 4 °C, with gentle agitation on a slow rotator unless noted otherwise. The decalcified inner ears were incubated in Image-iT fx (Molecular Probes, Eugene, OR) for 30 min. then transferred to blocking solution for 4 h at room temperature. Combinations of 2 or 3 primary antibodies were applied as a cocktail diluted in blocking solution, as described below, and incubated for 3 days. At the end of incubation, the samples were washed three times for 2 h each with PBS. The species-appropriate secondary antibodies were applied as a cocktail diluted in blocking solution and incubated for 3 days then washed three times with PBS for 2 h each. DAPI was included in the secondary antibody cocktail at a concentration of 0.25 μg/ml to label DNA. The monomeric cyanine DNA label To-Pro-3 was used on a few initial trial samples at 5 μM concentration in PBS for 45 min. following the final PBS wash after secondary antibody labeling.

2.3. Reagents

PBS – 0.2 M Na_2HPO_4, 0.075 M KH_2PO_4, 0.9% NaCl, pH 7.4.
Blocking solution – PBS containing 10% normal serum, 0.5% bovine serum albumin (A-7030, Sigma–Aldrich, St. Louis, MO), 0.1% Triton X-100 (Sigma–Aldrich).
Image-iT FX – Molecular Probes (Eugene, OR).
Normal goat serum – Vector Laboratories (Burlingame, CA).
Normal donkey serum – Jackson ImmunoResearch (West Grove, PA).
Methyl salicylate – Polysciences (Warrington, PA).
Benzyl benzoate – Fisher Scientific (Pittsburgh, PA).

Immunoreagents, with dilutions:

Anti-Parvalbumin – guinea pig polyclonal, 1/500 (Chemicon).
Anti-Parvalbumin – mouse monoclonal, 1/500 (Chemicon).
Anti-200 kD Neurofilament – rabbit polyclonal, 1/500 (Sigma).
Anti-Acetylated tubulin – mouse monoclonal, 1/250 (Sigma).
Donkey anti-mouse-Alexa488, 1/500 (Molecular Probes).
Goat anti-rabbit-Alexa568, 1/500 (Molecular Probes).
Donkey anti-guinea pig-Cy5 (Jackson ImmunoResearch).
DAPI – 0.25 μg/ml, with secondary antibodies (Sigma).
To-Pro-3 – 5 μM, post staining (Molecular Probes).

2.4. Dehydration and clearing

The washed samples were transferred to 70% ethanol for a period ranging from 2 h to overnight. Dehydration continued through 95% ethanol for 30 min, followed by two changes of absolute ethanol for 2 h each. The MSBB clearing agent was made by mixing

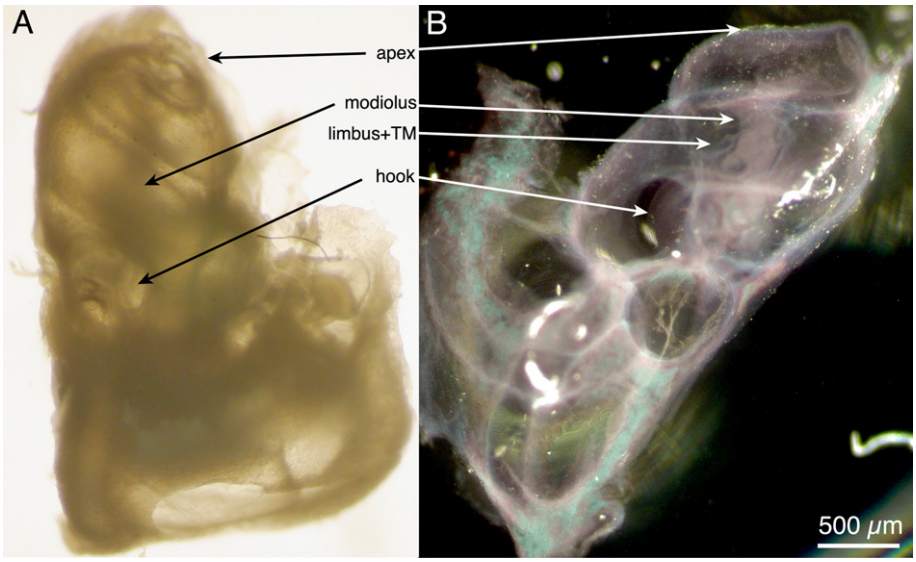

Fig. 1. The optical properties of the inner ear are dramatically altered by clearing in MSBB. (A) Shadows of the modiolus and pigmentation of the stria vascularis are the only internal structures visible from a non-cleared cochlea lying in PBS. 129/CBA mouse at P7. (B) A decalcified cochlea cleared in MSBB and imaged by oblique lighting clearly displays the modiolus, basilar lamina, spiral limbus and other structures. 129/CBA mouse, P33 days.

five parts methyl salicylate with three parts benzyl benzoate. Labeled inner ears were cleared in a 1:1 mixture of MSBB and absolute ethanol for 4 h followed by three changes of 100% MSBB for 2 h, 4 h and overnight, respectively. All clearing steps were carried at room temperature with gentle agitation on a platform rotator.

2.5. Epoxy embedding

A few labeled inner ears were examined on the confocal microscope for presence of labeling then rinsed free of MSBB by several changes of absolute ethanol over 24 h. MSBB was considered removed when the cochlea resumed the standard translucent appearance observed in absolute ethanol, prior to clearing. They were transferred from ethanol through two changes of propylene oxide for 60 min and 30 min, and then infiltrated overnight in a 1:1 mixture of propylene oxide and epoxy. After three changes of 100% epoxy for 30 min each, the samples were placed in a flat mold (#10504, Ted Pella, Inc., Redding, CA) and cured in a 60 °C oven until hardened (about 3 days). The epoxy was Spurr's Low Viscosity Embedding Resin using a modified formulation (Ellis, 2006) consisting of 23.60 gm nonenyl succinic anhydride, 7.60 g DER 736, 16.40 gm ERL 4221 and 0.1 g 2-(dimethylamino)ethanol (Electron Microscopy Sciences, Hatfield, PA). All steps were carried out at room temperature with agitation on a slow rotator.

2.6. Mounting

A cleared cochlea was placed on a silicone plate (Sylgard 184, K.R. Anderson Co., Morgan Hill, CA) and oriented on its medial side while viewed with a dissecting microscope (MZ-8, Leica Microsystems, Wetzlar, DE) using a combination of oblique illumination from a 150 W Techniquip fiberoptic illuminator (Livermore, CA) and darkfield illumination from the Leica stage. Imaging the organ of Corti by objectives with working distances over 500 μm only needed that the attached bone matrix or protruding semi-circular canals be trimmed so that the cochlea would lie flat and stable on the coverslip. Objectives with shorter working distances required that the side of the cochlear capsule be removed in order to position the organ of Corti within the objective's working distance. In this case, the cochlear shell was sliced in a paramodiolar plane, as shown in Fig. 2.

A specimen holder was created by using silicone aquarium sealant (All-Glass Aquarium Co., Franklin, WI) to affix a 24 mm × 50 mm coverslip of 170–173 μm thickness to a 25 mm × 75 mm × 1 mm aluminum frame that had supported PEN foils used for laser microdissection samples (Leica). This frame is made to the dimensions of a microscope slide and possesses a central opening of 15 mm by 40 mm. The specimen holder was used with the coverslip as the lower surface, facing the objective lens of an inverted microscope. The cochlea was placed on the coverslip so that it rested on its trimmed surface and was wetted with a small quantity of MSBB to prevent drying or entrapment of air bubbles within the sample or reflections. The frame supported the coverslip in a manner that reduced flexure and formed a barrier to prevent the MSBB from dripping onto the objective lens or other microscope components. No other covering or coverslip was needed. Occasionally, a small square cut from a coverglass was used as a shim under one side of the cochlea to prevent it from rolling.

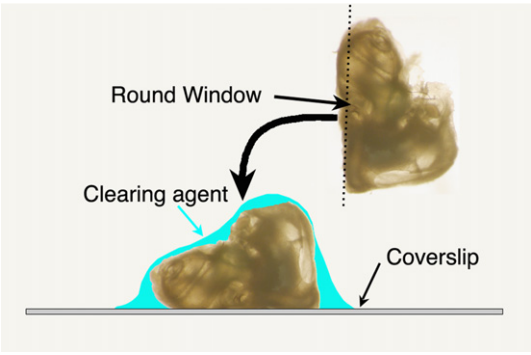

Fig. 2. The capsule may be trimmed to allow the cochlea to lie on the coverslip, or sliced (e.g., along the dashed line) to open the capsule to allow the organ of Corti to be viewed by high NA objectives with short working distances. The frame used to support the coverslip is not shown.

2.7. Sectioning

Epoxy embedded inner ears were bisected along the axis of the modiolus, as previously described (Hardie et al., 2004). Cross-sections from the exposed turns were cut at 2 μm thickness using a diamond Histoknife (Diatome AG, Biel, SW) and mounted on microscope slides subbed with chrome alum-gelatin. Sections intended for epi-fluorescent microscopy were coverslipped with Fluoromount G (Southern Biotech, Birmingham, AL). Adjacent sections were stained with Richardson's methylene blue and azure II (Richardson et al., 1960) then coverslipped with Fluoromount G.

2.8. Microscopy and image processing

Sections were imaged with an AxioPlan 2ie (Carl Zeiss) equipped with a Coolsnap HQ monochrome digital camera (Princeton Instruments, Trenton, NJ). The microscope and camera were controlled by Slidebook (Intelligent Imaging Innovations, Denver, CO), version 4.0.2.8, on a Macintosh G4 computer.

All confocal images were collected on a Fluoview-1000 laser scanning confocal microscope equipped with an IX-81 inverted microscope (Olympus America, Center Valley, PA). DAPI was excited by a 405 nm diode laser and its signal was detected through a 490 nm longpass dichroic and a 425–475 nm diffraction filter. Alexa 488 was excited by the 488 nm line from an argon ion laser, with signal directed by a 560 nm longpass dichroic mirror into a 500–550 diffraction filter. Alexa 568 was excited with a 561 nm solid state laser, separated by a 640 nm longpass dichroic mirror or front surface mirror, using a 575–625 interference filter. Far red fluorescent labels were excited with a 633 nm helium–neon laser, directed to the detector with a front surface mirror and through a 655–755 nm barrier filter. This study used the 4X/NA .16, 10X/NA .4 and 20X/NA .75 UPLSAPO dry objective lenses and a 40X/NA 1.3 UPLFL oil immersion objective lens.

Confocal images were acquired with 12-bit digitization and saved as 16-bit TIFF. Deconvolution using a maximum likelihood estimate algorithm was applied to all volumes using Huygens Essential 3.0.0 (Scientific Volume Imaging, Hilversum, NL) on a computer with two dual core Opteron processors (AMD, Sunnyvale, CA) running 64-bit Enterprise Linux (Redhat, Raleigh, NC). Maximum intensity projections (MIP) along the *z*-axis and MIP rotations were created using Huygens Essential and by ImageJ, version 1.38 (Rasband, W.S., ImageJ, US National Institutes of Health, Bethesda, Maryland, USA, http://rsb.info.nih.gov/ij/, 1997–2006). ImageJ was used on either a Macintosh dual G5, running OS 10.4.10 (Apple, Inc., Cupertino, CA) or on Enterprise Linux. Final figures were created with Adobe Photoshop version 9.0 on a Dual G5 Mac OS 10.4.10. All figures were subjected the minimum degree of histogram stretch and gamma adjustment necessary to maintain contrast during publication.

3. Results

A fixed, uncleared cochlea infiltrated with PBS and imaged through a dissecting microscope using transmitted light is nearly

opaque with shadows suggesting presence of internal structures (Fig. 1A). In contrast, a cochlea cleared by MSBB is nearly transparent when viewed under the same dissecting microscope using dark-field illumination from the Leica stereomicroscope stage. The oblique illumination from this mode allowed otherwise transparent internal structures to be clearly observed, such as the modiolus spiral limbus and tectorial membrane (Fig. 1B). Although a decalcified cochlea is quite soft, exposure to MSBB hardened the tissue sufficiently that it could be trimmed with minimal distortion prior to mounting on the sample holder coverslip, as demonstrated in Fig. 2.

Strong fluorescent signals were obtained throughout the full thickness of the cochlea. This allowed use of very low laser intensities to avoid photobleaching during the prolonged scanning required to acquire relatively deep image volumes and to minimize tissue autofluorescence. The time to acquire a z-stack was largely dependent upon the sampling density of the field and on the degree of axial resolution. An image stack sequentially capturing three channels with an 800×800 sampling density, 2 μs dwell time, without averaging, and incrementing focus at the Nyquist interval required 45–60 min. Smaller fields and reduced axial depths to view specific regions, such as the cochlear apex or a short interval organ of Corti in cross-section, required 15–25 min.

The Alexafluor conjugates tended to stick to the inner and outer surfaces of the cochlea and the tectorial membrane. This was greatly reduced by pre-treatment with the Image-iT FX reagent. Small, punctate, brightly fluorescent particles sometimes persisted in a few samples. The source of this artifact has not yet been determined. A low intensity non-specific fluorescence arising from the Alexafluor 568-conjugated antibody persisted in the tectorial membrane, Reissner's membrane and the basilar membrane within brightest point projections. This became noticeable after contrast enhancement to extract small features such as nerve fibers.

Each individual image plane displayed little background fluorescence within the organ of Corti, possibly due to the inherent high contrast from the dispersed arrangement of cell types. However, due to the depth of the optical volumes acquired, the cumulative effect of a low amount of out of focus light due to residual aberrations and scattering reduced overall contrast and masked small structures, as described above for the Alexafluor 568. Deconvolution proved to be essential to remove the out of focus light from these thick optical volumes in order to improve contrast and unmask details.

The organ of Corti could be imaged readily through the connective tissue of the decalcified shell and the stria vascularis by objective lenses with long working distance, as shown in Figs. 3 and 4, which were collected from the same cochlea. The outer connective tissue matrix of the cochlear capsule had little impact on the quality of images collected from deeper regions. However, it imparted a subtle haze over interior structures when the surface was included in maximum intensity projection (MIP) images (Fig. 3). In comparison, the same specimen is presented in Fig. 4 with a MIP restricted to the central 96 μm of the cochlea. The haze imparted by connective tissue of the bone is present only at the edges of the cochlear duct due to curvature of the structure. High levels of fluorescence in localized regions of the bone correspond to highly cellular marrow spaces.

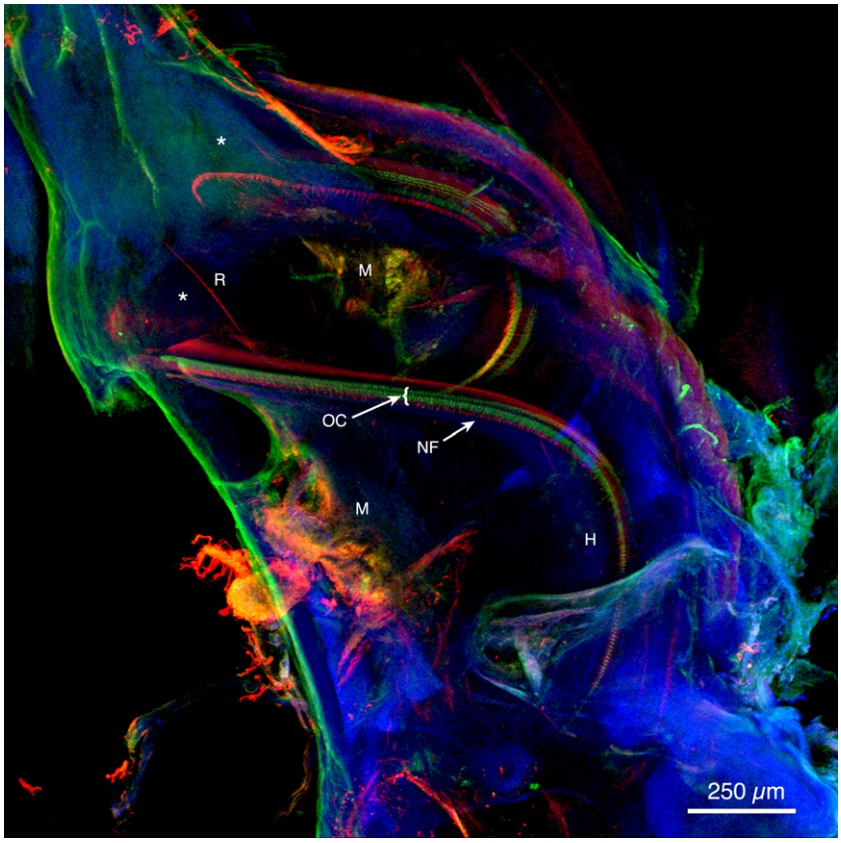

Fig. 3. A maximum intensity projection (MIP) from an intact mature mouse cochlea imaged through its entire volume. The organ Corti (OC) appears as a red and green ribbon (}) spiraling from the hook region (H) upwards to the apex. Nerve fibers (arrow) immunolabeled for 200 kD neurofilament (red) are present below the hair cells and traverse radially through the modiolar shelf toward the modiolus (M). Sensory hair cells immunolabeled for parvalbumin (green) appear sandwiched between the nerve fibers and non-specific red label in the tectorial membrane. The scala media (*) is outlined in first and second turns by Reissner's membrane (R), also red from non-specific labeling. The hook region may be observed curving around the round window. Image width is 1.988 mm, 856 μm volume thickness. 129/CBA mouse, P33 days, 4×/0.16 objective. Supplemental Figure 1 shows another example of a complete cochlea.

Opening the cochlea by trimming away the outer connective tissue and stria vascularis, as shown in Fig. 2, reduced the distance between the supporting coverslip and sensory epithelium. Fig. 5 presents the organ of Corti and modiolus collected from the upper turn, after opening the cochlea of the same cochlea presented Figs. 3 and 4. When viewed as separate channels, fine details are visible that are obscured when viewed as merged color images. Presumptive afferent nerve fibers labeled by 200 kD neurofilament (Berglund and Ryugo, 1991) in Fig. 5A (200 kD NF, red in inset and D) radiate from the modiolus while efferent fibers labeled for 200 kD NF (Maison et al., 2006) are visible in the intraganglionic spiral bundle (IGSB). Both types of fibers densely innervate the region of the IHC and cross the tunnel of Corti to the OHC. Parvalbumin in Fig. 5B (PARV, green in inset and D) labeled neurons in the spiral ganglion, the sensory hair cells, as well as thin, filamentous nerve fibers in the outer spiral bundle below the OHC. The arrangement and shape of nuclei in Fig. 5C, labeled by DAPI (blue in inset and D), may be used as anatomical landmarks for structures such as the elliptical nuclei in tympanic border cells of the basilar membrane (BM) and rows of inner dentate cells in the spiral limbus (SpL). The merged image in Fig. 5D shows the relative positions of the most prominently labeled structures. The inset was created by a MIP of a 3 μm thick "vertical slice" extracted in the *YZ* dimension from the center of the volume.

Another example of the impact of the dense connective tissue of the bone is shown in Fig. 6, which contains the same cochlea is shown in Figs. 3–5, but rolled 90° onto its lateral side with its apex pointed towards the objective lens. A large piece of cochlear shell removed from the apex during the initial dissection allowed an unobstructed view along the modiolar axis. Nuclear staining and background fluorescence of the stria vascularis and connective tissues of the lateral wall did not obscure a view of the spiraling cochlear duct. However, portions of dense connective tissue of the bone along the top of the image and the lower left corner (*) reduce contrast in the underlying tissues. Spiral ganglion neurons were intensely labeled for parvalbumin at the very tip of the modiolus and the opening at the base of the modiolus, where the cells were accessible to the antibodies.

The paths taken by afferent fibers are shown in Fig. 7, a volume collected from an opened cochlea taken from a littermate to the previous figures. The apparent shapes of the IHC and OHC differ between Figs. 5 and 7 due to orientation of the cochlea on the supporting coverslip. A mix of nerve fibers, predominately labeled for 200 kD neurofilament (red), with some fibers labeled for parvalbumin (green), constrict to pass through the habenula perforata then spread out. Some neurofilament labeled fibers emerge from the habenula and appeared to travel laterally for varying distances in the inner spiral bundle before crossing the tunnel (arrowheads).

The image volume presented in Fig. 7 was cropped to remove the basilar membrane and the supra-nuclear portions of the OHC. This OHC basal region is presented in Fig. 8 with each panel representing the MIP of six consecutive image planes acquired at 0.5 μm intervals. Stepping through this sub-volume allowed close observation of the arrangement of nerve fibers and synapses as individual OHCs came into focus. The OHCs and nerve fibers in the outer spiral bundle were labeled for parvalbumin (green) while 200 kD neurofilament (red) labeled possible efferent fibers. Fig. 8A is below the bases of the OHC and as each subsequent panel advances 3 μm towards the cuticular plate additional OHCs and innervations came into focus. The outer spiral fibers display periodic swellings that may indicate the proximity of synapses and with some synapses visible on OHCs (arrowheads). The putative efferent fibers were also observed to form synapses (arrows) on the OHCs, with cells possessing synapses from both types of fibers in Fig. 8C and D.

Use of an antibody against acetylated tubulin presented a striking image of its distribution within pillar cells and Deiters' cells (Fig. 9B and D). The inner and outer pillar cells were filled with labeled microtubules from the footplate structure to the reticular

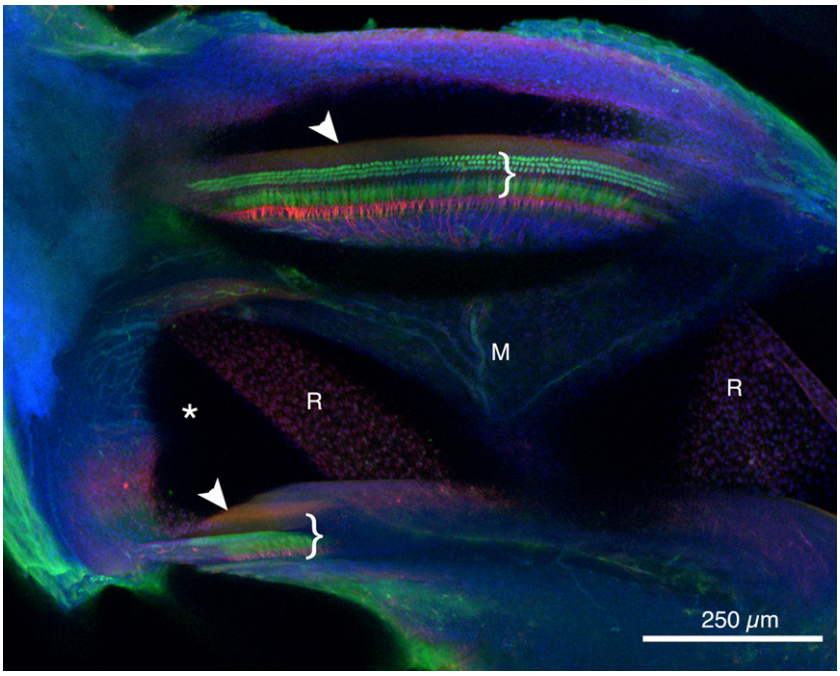

Fig. 4. A view near the center of the inner ear presented in Fig. 3, prior to slicing open the cochlear capsule. This volume began 400 μm from the coverglass. The IHCs and OHCs, labeled for parvalbumin (green) appear in the upper turn with a stereotypical arrangement in cross-section (bracket) but appear merged in the lower turn due to curvature of the organ of Corti. Nerve fibers labeled for 200 kD neurofilament (red) radiate from the modiolus (M) and emerge from the habenula perforata as a densely labeled border below the IHC. A few tunnel crossing fibers continuing outwards to the OHC are observed at this magnification. The tectorial membrane is identified by non-specific label from the Alexafluor 568 (arrowheads). Reissner's membrane (R) is clearly visible demarcating the scala media (*) in the lower turn. MIP from 96 μm volume thickness, 129/CBA mouse, P33 days, 10×/0.40 objective.

lamina (Angelborg and Engstrom, 1972; Slepecky et al., 1995). However, each Deiters' cell was identified by a pair of dense bundles of microtubules originating at a bifurcation (lower arrows, Fig. 9B) above the footplate process. One bundle led to the base of an OHC and the other bundle, the phalangeal process, rose to the reticular lamina, as described in gerbil and guinea pig (Angelborg and Engstrom, 1972; Slepecky et al., 1995). The phalangeal processes also bifurcated as they approached the reticular lamina (upper arrow, Fig. 9B). The presence of acetylated tubulin in outer spiral fibers (Hallworth and Ludeuna, 2000) is barely visible through the large structures of the tubulin bundles in the pillar cells and phalangeal processes of the Deiter's cells (arrowheads). Nerve fibers labeled with 200 kD neurofilament are observed forming synapses on the bases of hair cells (arrows, Fig. 9A), correlating with the images in Fig. 8. Parvalbumin stained the OHC and synapses (arrowheads, Fig. 9C) from longitudinal fibers in the outer spiral bundle, resembling the synapses in Fig. 8. The anti-parvalbumin antibody was labeled with a far red fluorophore which was pseudocolored in the blue channel of the color merge panel (Fig. 9D). The blue channel displays parvalbumin with low intensity in order to maintain the visibility of the 200 kD neurofilament (red) and acetylated tubulin (green).

Semi-thin sections were collected from an inner ear that had been processed for immunolabeling, cleared in MSBB and then embedded in Spurs' low viscosity resin. These sections presented typical cross-sectional views of the organ of Corti when viewed by transmitted light DIC, Fig. 10A and C. Epi-fluorescence images from adjacent sections, Fig. 10B and D, resembled conventional fluorescent images obtained by methods such as frozen sections. However, although the immunolabeling for parvalbumin (green) clearly labeled IHC, OHC and nerve fibers, the regions of connective tissue were of equal intensity. Similarly, regions of the spiral limbus and areas such as the spiral ligament expressed a far red fluorescence that obscured the nuclei labeled with To-Pro-3 (pseudocolored red) and the plastic itself displayed moderate levels of autofluorescence.

4. Discussion

This report extends our prior work to obtain 3D images of the intact mammalian inner ear that used embedding in Spurr's low viscosity resin (Hardie et al., 2004) as a clearing mechanism. The confocal volumes in that report were limited by loss of signal and resolution to focus depths that were much less than the working distance of our objective lenses. In addition, we recently encountered several problems from changes in the available components for Spurr's resin, even when used in new formulations (Ellis, 2006). Use of MSBB as a clearing agent to avoid embedding in Spurr's resin provided a dramatic improvement in image quality.

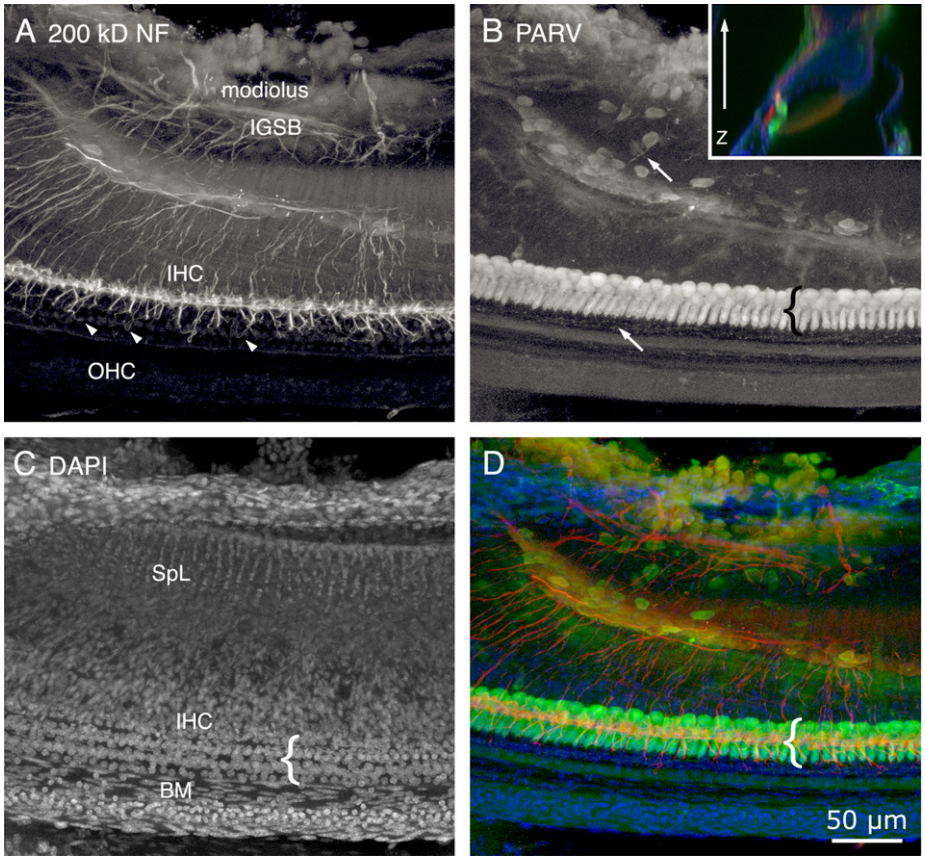

Fig. 5. The upper turn from the previous two figures was imaged after opening the cochlea and is displayed as separate channels. (A) Afferent fibers labeled for 200 kD neurofilament (red, inset and D) travel from the spiral ganglion, at top, and pass below the spiral limbus (unlabeled) to aggregate below the IHC region. Labeled efferent fibers travel longitudinally in the intraganglionic spiral bundle before turning towards the organ of Corti. The tunnel crossing fibers pass across the tunnel of Corti and form a characteristic hook as they veer near the basilar membrane before turning upwards to the bases of the OHC (arrowheads). (B) Parvalbumin (green, inset and D) is observed in hair cells, spiral ganglion neurons and some thin nerve fibers in the modiolus and outer spiral bundles (arrows). (C) Patterns of DAPI-labeled nuclei (blue, inset and D) indicate the locations several landmark features such as the hair cells and rows of nuclei in the dentate cells of the spiral limbus (SpL). The elliptical nuclei in the tympanic border cells in the basilar membrane (BM) are observed through the distal support cells. (D) The color merge of panels A, B and C. The inset is a MIP from the YZ plane to indicate the orientation of the organ of Corti relative to the axis of focus (objective lens at lower edge). MIP from 231 µm thickness, 129/CBA mouse, P33 days, 20×/.75 objective. Supplemental Fig. 2 further illustrates the curvature of the radial fibers as they approach the OHC.

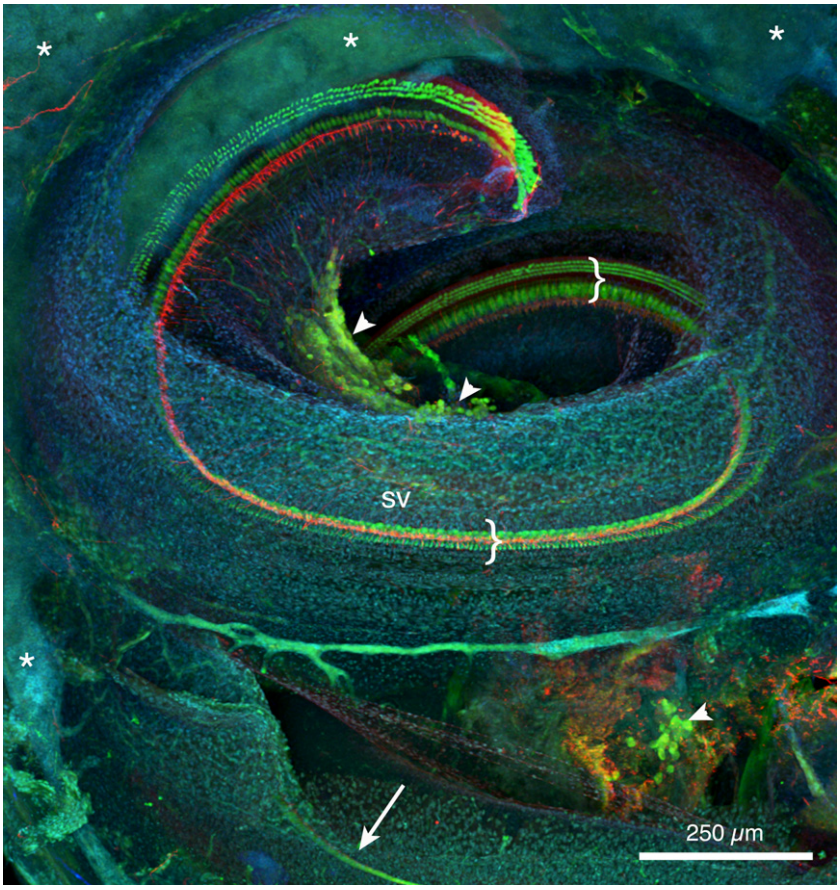

Fig. 6. An oblique view from the same cochlea shown in Figs. 3–5, re-oriented onto its lateral side, with the apex angled towards the coverslip. The cochlear duct and sensory cells (}) spiraling around the modiolar axis are readily visible through the constellation of nuclei in the stria vascularis (sv) and lateral wall tissue. Both IHC and OHC are labeled for parvalbumin (green) and nerve fibers are labeled for 200 kD neurofilament (red). In contrast, the dense connective tissue of the bony shell (*) obscures underlying tissues. The basal turn may be observed as it passes near the round window (arrow). Neurons of the spiral ganglion are labeled for parvalbumin (arrow heads) at both the apex and base of the modiolus. MIP from 651 μm volume thickness, 129/CBA mouse, P33 days, 10×/0.40 objective. Supplemental Fig. 3 steps through the z-series to demonstrate label penetration through the volume. Supplemental Fig. 4 presents a rotating MIP of this volume.

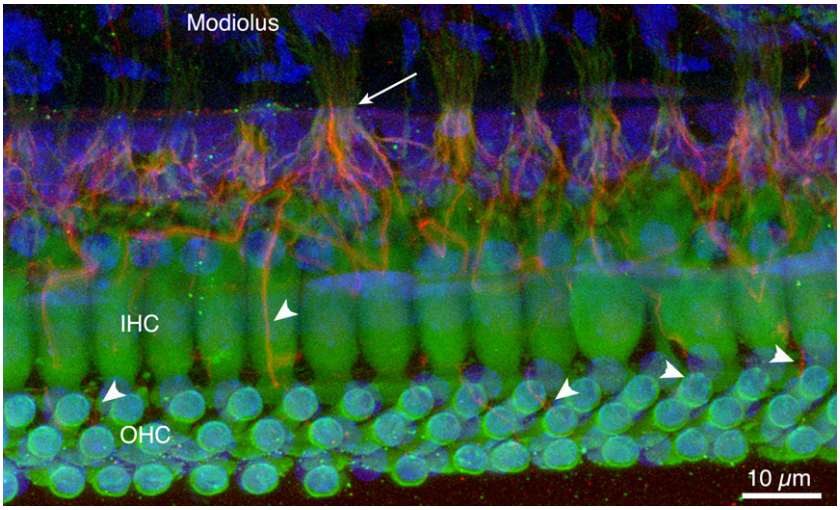

Fig. 7. Hair cells labeled for parvalbumin (green) appear in nearly opposite orientations, OHC are oriented nearly perpendicularly to the plane of focus, while the IHC are nearly parallel. Bundles of nerve fibers labeled for 200 kD neurofilament (red) and for parvalbumin constrict to pass through the habenula perforata. Some fibers labeled for 200 kD neurofilament appear to follow the inner spiral bundle for short distances before crossing the tunnel of Corti (arrowheads) to innervate the OHC. 129/CBA mouse, P33 days, 40×/NA1.3 oil immersion objective.

The cochlea contains many different structures ranging from dense connective tissues to large open chambers, each with its own refractive index (RI). The cochlear shell remains quite visible in common mountants for fluorescent imaging, which have an RI in the range of 1.44–1.49, and therefore is not matched by these lower RI values. The improved depth of focus made possible by

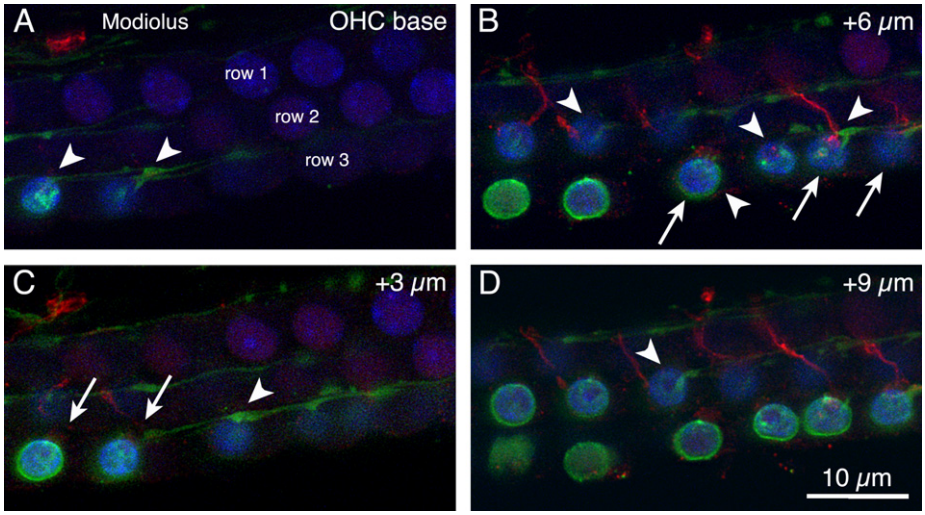

Fig. 8. A series of maximum intensity projections (MIPs) in the basal OHC region cropped from the volume in Fig. 7. Each panel is a MIP from a 3 μm layer (six image planes) progressing towards the cuticular plate. (A) The initial plane shows thin longitudinally arranged fibers labeled by parvalbumin (green) forming teardrop shaped swellings as they approach the OHC bases to form synapses (arrowheads). Each fiber forms large synapses on multiple cells. (B) This MIP is 3 μm closer towards the cuticular plate and synapses appear on the middle row of OHC. Possible efferent fibers labeled by neurofilament (red) appear to form synapses (arrows). Additional synapses of both types appear on the same cells in C and D. 129/CBA mouse, P33 days, 40×/1.30 oil immersion.

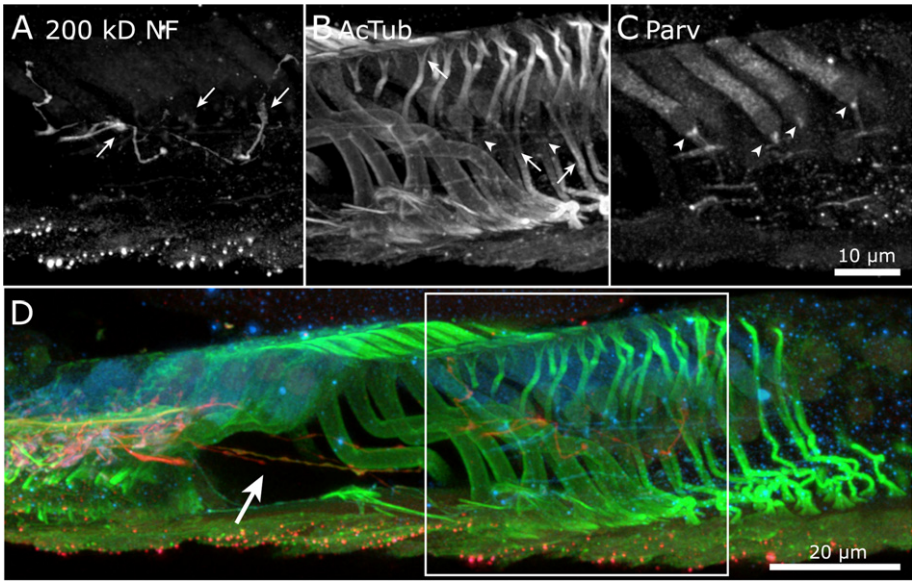

Fig. 9. A volume collected approximately 180° from the apical terminus of the organ of Corti is presented as separate channels (A–C) and as a merged image (D). (A) Possible efferent tunnel crossing fibers labeled for 200 kD neurofilament form synapses on the OHC (arrows). (B) Acetylated tubulin labels large fiber bundles filling the pillar cells from the basilar membrane to the reticular lamina. A thinner bundle in each Dieters cell bifurcates (lower arrows) above a footplate on the basilar lamina and again (upper arrow) below the reticular lamina. Nerve fibers faintly labeled pass through the support cells (arrowheads). (C) Parvalbumin labels both OHC and nerve fibers in the outer spiral bundle. Synapses (arrowheads) are indicated by strong staining at the base of each OHC. (C). (D) The color merge of all three channels obscures some details (neurofilament = red, acetylated tubulin = green, parvalbumin = blue). Efferent fibers (large arrow) appear labeled for combinations of acetylated tubulin and neurofilament. The square outline defines the region presented as separate channels in panels A–C. 129/CBA mouse, P28 days, 20×/.75 objective lens, 42 μm volume depth, 150 μm from the coverslip.

MSBB is most likely due to its RI of 1.556 being a closer match to the RI of cochlear tissues than was the RI of epoxy resin. Mixtures of benzyl benzoate, methyl salicylate and other organic reagents have been used since at least the 19th century to create clearing agents with RI matched to specific tissues in order to render them transparent (Spalteholz, 1914). MSBB has been used previously to render the mammalian inner ear optically transparent (Voie et al., 1993) for macroscopic imaging utilizing a camera lens with relatively low numerical aperture (NA).

Microscope objective lenses are designed for specific conditions, including a uniform sample refractive index and a specific coverslip thickness (Keller, 2006). Deviations from these design conditions produce degraded images by spherical aberration. Spherical aberration occurs at each RI interface because high angle light rays from the margins of a lens refract more than the paraxial rays at the center of the lens (Born and Wolf, 2005). This causes the light rays to be focused at multiple levels within the sample to create images that suffer from reduced intensity and degraded resolution.

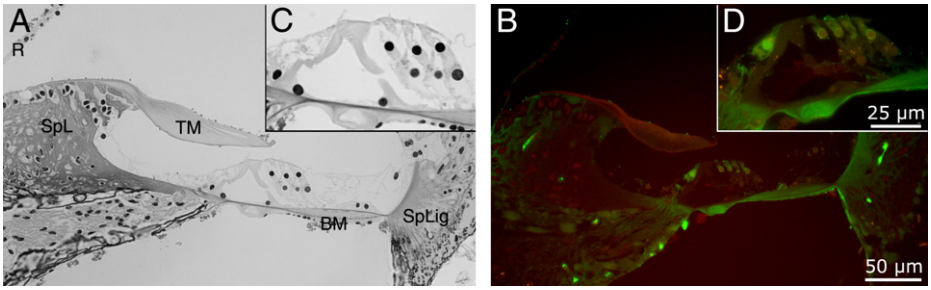

Fig. 10. Semi-thin sections, 2 µm thickness, from an inner ear embedded in Spurr's resin after immunolabeling and clearing in MSBB. A typical transverse section through the organ of Corti stained by Richardson's stain at 20× (A) and 63× (C) with DIC optics. An adjacent section viewed by epi-fluorescence at 20× (B) and at 63× (D) displays high levels of non-specific fluorescence in the spiral limbus (SpL), tectorial membrane (TM), spiral ligament (SpLig), basilar membrane (BM) and Reissner's membrane (R) as well as within the epoxy. Hair cells and nerves are labeled for parvalbumin (green) and for DNA by To-Pro-3 (red). 129/CBA mouse, P6 months. 20×/.75 Plan-Apochromat objective lens (A–B), 63×/1.4 oil immersion Plan-Apochromat (C–D).

Spherical aberration increases commensurate with depth of focus relative to the coverglass and becomes more significant with high NA objectives (Carlsson, 1991; Hell et al., 1993; Torok et al., 1997; Egner and Hell, 2006). Backscatter of excitation and fluorescent emissions at these interfaces additionally contributes to loss of signal intensity and contrast. Deviation from the recommended coverslip thickness also increases the spherical aberration. Use of a coverslip close to the 170 µm required for our lenses and an immersion oil matching the RI of MSBB further reduced RI variations and spherical aberration in our samples.

We removed the MSBB from cleared inner ears by absolute ethanol to test whether such specimens could be embedded in epoxy resin to obtain correlative sections. We did not investigate whether MSBB was sufficiently soluble with epoxy resin that it could be used as a transitional solvent. Unfortunately, while standard brightfield sections were possible (Fig. 10A and C), the current Spurr's resin formulation exhibited high autofluorescence when viewed by fluorescent microscopy (Fig. 10B and D). Other resins, such as Araldite and epon replacements may be compatible with pre-embedding immunofluorescent labeling of the inner ear, although extended infiltration times will be required due to higher viscosity.

The long incubations for antibody penetration and holes dissected in the middle turns were essential to allow solution exchange. Without dissection, if labeling occurred, it was only near the openings at the round window and the apex. Further refinements should be explored to reduce the length of time required to reduce preparation time and to improve antibody penetration. Microwave processing during decalcification (Tinling et al., 2004) or during the incubations with primary and secondary antibodies (Munoz et al., 2004) may be useful.

The image volume sizes obtained by this method were constrained by the working distance of the objective rather than section thickness or spherical aberration, as with most section-based preparations. The interplay of axial and lateral sampling densities and field size needed to be carefully balanced to provide the required degree of resolution while avoiding photobleaching and overwhelming computational capabilities (Hibbs et al., 2006). Attempting to collect multi-channel images at the full resolution of any objective over its full field of view could easily generate image files up to 3 gigabytes and require hours to acquire.

The antibodies used in this project were selected to provide an overview of cochlear histology while exploring the limits of this method. Although the calcium binding protein parvalbumin has been demonstrated to be present within the neuronal somata of both the spiral ganglion and the olivocochlear nuclei (Celio, 1990), it has not been previously shown in nerve fibers below the OHC. This may be due to differences in the specificity of antibodies employed, as has been discussed for other immunocytochemical studies of the inner ear (Slepecky and Ulfendahl, 1992). The parvalbumin-labeled nerve fibers described here resemble afferent fibers by their shape and small size, as well as the shape and arrangement of their synapses on the OHC (Sato et al., 1999; Berglund and Ryugo, 1987). However, positive identification will require further immunolabeling studies with combinations of specific antibodies, particularly those targeting pre- and post-synaptic proteins. Afferent fibers from the Type I and Type II neurons in the spiral ganglion in mice have been labeled by several antibodies against 200 kD neurofilament (Berglund and Ryugo, 1991). Efferent fibers innervating the mouse OHC also label for 200 kD neurofilament (Maison et al., 2006). As with our labeling for parvalbumin in longitudinally oriented fibers, confirming the identity of the fibers forming synapses on the OHC will require additional immunolabeling studies with multiple labels for 200 kD neurofilament, neurotransmitters and pre-synaptic proteins (Maison et al., 2003, 2006) or peripherin (Huang et al., 2007).

5. Summary

The ability to generate 3D images from intact cochlea presents many advantages over serial reconstruction. The time required for hands-on attention to sample preparation, image acquisition and image processing are greatly reduced. The process of aligning serial sections and errors from lost or misplaced sections are avoided. This method may allow spatial relations to be mapped, quantified and related to volumetric images from other studies or from other 3D methods such as MRI. Mapping 3D distributions of markers or gene expression as overlays promises to add multiple dimensions to our understanding of the development and biology of the mammalian cochlea.

Acknowledgements

Mae del Puerto provided expert technical assistance for dissections and labeling. We wish to thank Dr. Olivia Birmingham-McDonogh for use of the image of the P7 cochlea. Dr. Elizabeth Oesterle and Dr. Staci Sorenson provided insight and discussion. Mice were provided by Dr. Bronya Keats.

This work was supported by NIDCD grants DC04661 and DC03829, and the Foundation Fighting Blindness BR-GE-0606-0347.

Fig. 6 was awarded 2nd place in the 2007 Bioscapes digital imaging competition sponsored by Olympus, and was published in Scientific American, December, 2007.

Appendix A. Supplementary data

Supplementary data associated with this article can be found, in the online version, at doi:10.1016/j.heares.2008.05.009.

References

Angelborg, C., Engstrom, H., 1972. Supporting elements in the organ of Corti. I. Fibrillar structures in the supporting cells of the organ of Corti in mammals. Acta Otolaryngol. 301 (Suppl.), 49–56.

Benveniste, H., Blackband, S., 2002. MR microscopy and high resolution small animal MRI: applications in neuroscience research. Prog. Neurobiol. 67, 393–420.

Berglund, A.M., Ryugo, D.K., 1987. Hair cell innervation by spiral ganglion neurons in the mouse. J. Comp. Neurol. 255, 560–570.

Berglund, A.M., Ryugo, D.K., 1991. Neurofilament antibodies and spinal ganglion neurons of the mammalian cochlea. J. Comp. Neurol. 306, 393–408.

Born, M., Wolf, E., 2005. Principles of Optics, seventh ed. Cambridge, New York.

Carlsson, K., 1991. The influence of specimen refractive index, detector signal integration, and non-uniform scan speed on the imaging properties in confocal microscopy. J. Microsc. 163, 167–178.

Celio, M.R., 1990. Cabindin D-28k and parvalbumin in the rat nervous system. Neuroscience 35, 375–475.

Egner, A., Hell, S.W., 2006. Aberrations in confocal and multi-photon fluorescent microscopy induced by refractive index mismatch. In: Pawley, J.B. (Ed.), Handbook of Biological Confocal Microscopy, third ed. Springer, New York, pp. 404–441.

Ellis, E.A., 2006. Solutions to the problem of substitution of ERL 4221 for vinyl cyclohexene dioxide in Spurr low viscosity embedding formulations. Microsc. Today 14, 32.

Hallworth, R., Ludeuna, R.F., 2000. Differential expression of β tubulin isotypes in the adult gerbil cochlea. Hear. Res. 148, 161–172.

Hardie, N.A., MacDonald, G., Rubel, E.W., 2004. A new method for imaging and 3D reconstruction of mammalian cochlea by fluorescent confocal microscopy. Brain Res. 1000, 200–210.

Hashimoto, S., Kimura, R.S., Takasaka, T., 1990. Computer-aided three-dimensional reconstruction of the inner hair cells and their nerve endings in the guinea pig cochlea. Acta Otolaryngol. 109, 228–234.

Hell, S., Reiner, G., Cremer, C., Stelzer, E.H.K., 1993. Aberrations in confocal fluorescence microscopy induced by mismatches in refractive index. J. Microsc. 169, 391–405.

Hibbs, A.R., MacDonald, G., Garsha, K., 2006. Practical confocal microscopy. In: Pawley, J.B. (Ed.), Handbook of Biological Confocal Microscopy, third ed. Springer, New York, pp. 650–671.

Huang, L-C.L.-C., Thorne, P.R., Housley, G.D., Montegomery, J.M., 2007. Spatiotemporal definition of neurite outgrowth, refinement and retraction in the developing mouse cochlea. Development 134, 2925–2933.

Keller, H.E., 2006. Objective lenses for confocal microscopy. In: Pawley, J.B. (Ed.), Handbook of Biological Confocal Microscopy, third ed. Springer, New York, pp. 154–161.

Liberman, M.C., Dodds, L.W., Pierce, S., 1990. Afferent and efferent innervation of the cat cochlea: quantitative analysis with light and electron microscopy. J. Comp. Neurol. 301, 443–460.

Maison, S.F., Adams, J.C., Liberman, M.C., 2003. Olivocochlear innervation in the mouse: immunocytochemical maps, crossed versus uncrossed contributions and transmitter colocalization. J. Comp. Neurol. 455, 406–416.

Maison, S.F., Rosahl, T.W., Homanics, G.E., Liberman, M.C., 2006. Functional role of GABAergic innervation of the cochlea: Phenotypic analysis of mice lacking $GABA_A$ receptor subunits α1, α2, α5, α6, ß2, ß3, or delta. J. Neurosci. 26, 10315–10326.

Munoz, T.E., Giberson, R.T., Demaree, R., Day, J.R., 2004. Microwave-assisted immunostaining: a new approach yields fast and consistent results. J. Neurosci. Meth. 137, 133–139.

Richardson, K.C., Jarret, L., Finke, E.H., 1960. Embedding in epoxy resins for ultrathin sectioning in electron microscopy. Stain Tech. 35, 313–323.

Sato, M., Henson, M.M., Henson, O.W., Smith, D.W., 1999. The innervation of outer hair cells: 3D reconstruction from TEM serial sections in the Japanese macaque. Hear. Res. 135, 29–38.

Slepecky, N., Ulfendahl, M., 1992. Actin-binding and microtuble-associated proteins in the organ of Corti. Hear. Res. 57, 201–215.

Slepecky, N., Henderson, C.G., Saha, S., 1995. Post-translational modifications of tubulin suggest that dynamic microtubules are present in sensory cells and stable microtubules are present in supporting cells of the mammalian cohlea. Hear. Res. 91, 136–147.

Spalteholz, W., 1914. Über das Durchsichtigmachen von menschlichen und tierischen Präparaten und seine theoretischen Bedingungen. Hirzel, Leipzig.

Tinling, S.P., Giberson, R.T., Kullar, R.S., 2004. Microwave exposure increases demineralization rate independent of temperature. J. Microsc. 215, 230–235.

Torok, P., Hewlett, S.J., Varga, P., 1997. The role of specimen-induced spherical aberration in confocal microscopy. J. Microsc. 188, 158–177.

Voie, A.H., Burns, D.H., Spelman, F.A., 1993. Orthogonal-plane fluorescence optical sectioning: three-dimensional imaging of macroscopic biological specimens. J. Microsc. 170, 229–236.

Voie, A.H., 2002. Imaging the intact guinea pig tympanic bulla by orthogonal-plane fluorescence optical sectioning microscopy. Hear. Res. 171, 119–128.

Voie, A.H, Saxon, G., Hess, M., 2007. OPFOS imaging of the cochlea. Abstract, 30th Midwinter Research Meeting of the Assoc. for Res. in Otolaryngology, February 10.

Wang, G., Vannier, M., 2001. Micro-CT scanners for biomedical applications: an overview. Adv. Imag. 16, 18–27.